A SEM/FEM weak coupling for a more accurate definition of seismic input excitation in soil-structure interaction studies: An adaptation for a massively parallel FEM resolution

Michail Korres, Vinicius Alves Fernandes, Zentner Irmela, Nicolas Tardieu, François Voldoire, Filippo Gatti, Fernando Lopez-caballero

A SEM/FEM weak coupling for a more accurate definition of seismic input excitation in soil-structure interaction studies: An adaptation for a massively parallel FEM resolution

Journal of Physics: Conference Series **2647** (2024) 082008 doi:10.1088/1742-6596/2647/8/082008

A SEM/FEM weak coupling for a more accurate definition of seismic input excitation in soil-structure interaction studies: An adaptation for a massively parallel FEM resolution

M Korres[1], V Alves Fernandes[1], I Zentner[1], N Tardieu[1], F Voldoire[1], F Gatti[2] and F Lopez-Caballero[2]

[1]Electricité de France R&D, 7, Boulevard Gaspard Monge, 91120 Palaiseau, France
[2]Université Paris-Saclay, CentraleSupélec, ENS Paris-Saclay, CNRS, LMPS - Laboratoire de Mécanique Paris-Saclay, 91190, Gif-sur-Yvette, France

E-mail: michail.korres@edf.fr

Abstract. Numerical simulation of source-to-structure wave propagation consists of a challenging and demanding task in terms of computational capabilities and resources. Some difficulties related to the multi-scale character of the numerical problem can be alleviated using a spectral element (SEM) and finite element (FEM) weak coupling, such as the one described and verified in this study. In addition, the adaptation of the FEM resolution in a domain decomposition framework is developed allowing to utilize iterative solvers and ensure the scalability of the numerical solution in a High-Performance Computing (HPC) framework more efficiently. Comparisons with solutions adopting a direct parallel solver allow to demonstrate the important acceleration of the computation chain.

1. Introduction

Dynamic soil-structure interaction (SSI) studies are widely used in geotechnical earthquake engineering to evaluate structural capacity and component safety requirements under seismic loading. Given the uncertainties and physical complexity of the seismic excitation and the soil domain, as well as computational constraints, very often soil-structure interaction studies are bounded to vertically incident plane-waves and horizontal soil stratification assumptions. However, these simplifications may not be always adapted to all site conditions and seismic scenarios. In order to tackle this issue, the domain reduction method (DRM) proposed by [1] is considered in this work. It consists of a two-steps weak coupling approach where the complete 3D wave field obtained from an auxiliary domain is replaced by equivalent nodal forces to be exerted on the boundary surface of a reduced domain, providing a realistic definition of the seismic excitation.

In this framework, the complete problem can be decoupled and solved in two separate models with adapted numerical approaches. Therefore, an auxiliary domain defined on a regional scale integrating the seismic source and wave propagation from the source to the site of interest is proposed. This first step is solved in a spectral element framework (SEM), which is adapted for large-scale wave propagation studies. By obtaining the equivalent nodal forces on the boundary

surface of a reduced finite element model (FEM), soil-structure interaction analysis studies can be conducted integrating all the relevant aspects from source and path characteristics of a given seismic scenario. Consequently, the "incompatibility" of the different scales of the problem (regional, local) can be efficiently solved, by maintaining a sufficiently sophisticated numerical model for the local scale, where the hypothesis of a nonlinear soil behavior may be for instance examined.

The validation of the coupling is discussed in [2], while this work focuses on the performance of the second step of the coupling approach and the FEM resolution. The main objective is to present the feasibility of the FEM resolution with the DRM excitation in a high-performance computing (HPC) framework with code_aster [3]. In this context, the adaptation of the code is presented in a domain decomposition framework allowing to more efficiently utilise computational resources, make profit of iterative solvers and thus ensure the scalability of the numerical solution [4, 5, 6]. For demonstration purposes, the case-study of the Kashiwazaki-Kariwa nuclear power plant (KKNPP) at the region of Niigata in Japan is considered. This case was extensively studied by several authors [7, 8, 9, among others] but in this work serves as a simple study to quantify the numerical performance relative to the traditional use of direct parallel solvers. For this purpose, comparisons are also made with customary approaches utilizing direct parallel solvers. Finally, it is worth mentioning that HPC capabilities using the domain decomposition framework are already implemented in the SEM code SEM3D [10, 11].

This paper is organized as follows: Section 2 provides a brief description of the DRM methodology and the coupling procedure between the SEM-FEM software. Main aspects from the KKNPP case-study and a brief numerical verification of the SEM-FEM coupling are provided in Section 3. Finally, the newly implemented code_aster version for a massively parallel resolution with FEM is provided in section 4, before providing some general conclusions of the work.

2. Methods

This section provides the key ideas of the coupling procedure. The DRM approach as it was proposed by Bielak et al. [1], is discussed in the first part. Then the specifics of the SEM-FEM coupling based on the chosen numerical tools are provided in the second and last part of this section. For a more detailed description of the specific SEM-FEM coupling between the two software, the reader should refer to [2].

2.1. Domain Reduction Method (DRM)

The key concept of the DRM approach lies in the definition of a complex 3D incident wave field to be imposed as an input excitation to the reduced domain model [1]. In this framework, the objective of the DRM is to transfer the dynamic excitation of the seismic source closer to the boundaries of a reduced (smaller) domain of interest, at the scale of the site/structure.

For this purpose, source-to-structure wave propagation is considered in two separate steps, where the initial domain of interest Ω, is divided in two sub-domains by a virtual boundary surface Γ: i) the interior domain Ω_s, and ii) the exterior domain Ω'_s (Fig 1a). The wave propagation problem is then solved in two separate steps:

(i) **Auxiliary domain problem** $\mathcal{P}_0$: Local features of interest (*e.g.* complex geology, structures, *etc.*) are replaced by a simpler soil profile in continuation of the soil in depth (see Fig. 1b), and source-to-site propagation in the whole domain ($\Omega'_s \cup \Omega^0_s$) is performed in order to define the corresponding ground motion at the boundary (Γ) of an interior domain. Given the higher wave velocity of the soil a coarser mesh discretization can be chosen, leading to a faster source-to-site simulation.

(ii) **Reduced domain problem** $\mathcal{P}_r$: The second step considers only the reduced ($\Omega_s \cup \Omega_{snl}$) domain and the local features of interest are explicitly accounted for (see Fig. 1c). The

input excitation expressed in terms of equivalent nodal forces obtained directly from $\mathcal{P}_0$ and applied on the so-called DRM boundary Γ in a region that is slightly bigger than the local reduced domain. The soil outside the boundary Γ is only used for absorbing the diffracted waves traveling out of the domain and incompatible with $\mathcal{P}_0$ solution.

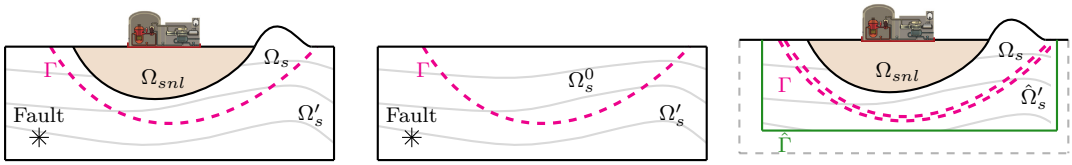

(a) Problem of reference. (b) Auxiliary domain problem. (c) Reduced domain problem.

Figure 1: Schematic representation of the domain reduction method (adapted from [1]).

It can be derived from the aforementioned description that the two key components that must be taken into account for the DRM are: i) a suitable absorbing boundary condition around the reduced domain, and ii) the definition of the equivalent nodal forces on a region in the reduced domain boundary. In this framework, the adopted solution for the SEM-FEM coupling utilises paraxial elements [12], a boundary condition already implemented in code_aster, allowing to absorb outgoing waves, as well as to apply the dynamic excitation.

2.2. SEM-FEM Coupling description

Provided the paraxial element formulation, the necessary fields that need to be considered in order to properly reconstruct the transient dynamic excitation at the boundary of the reduced domain are : i) the traction vector, and ii) the incident wave velocity field. For a more detailed demonstration the reader should refer to [2, 12, 13, 9].

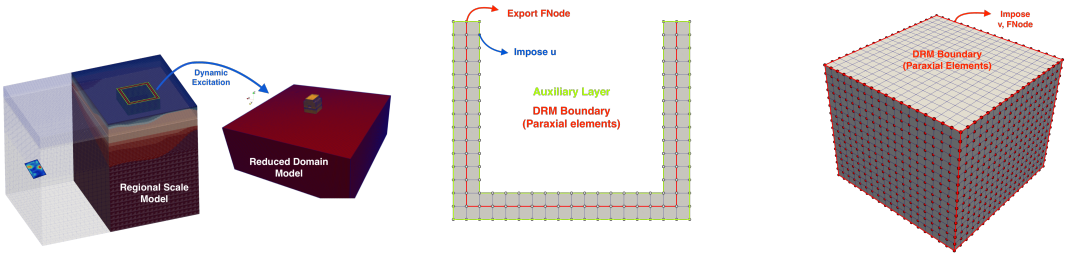

(a) Regional domain. (b) FEM Auxiliary layer. (c) Reduced domain.

Figure 2: Schematic representation of the coupling procedure between SEM3D and code_aster (reprinted from [2]).

A schematic representation of the coupling between SEM and FEM is presented in Fig. 2 and the procedure of field transfer is executed as follows:

(i) Define the surface boundary of the DRM interface Γ and the neighboring auxiliary layer in SEM domain (Fig. 2a). This step corresponds to the auxiliary domain problem $\mathcal{P}_0$.

(ii) Export displacement and velocity fields $(\mathbf{u}, \dot{\mathbf{u}})$ on predefined sensor points on GLL points lying on the DRM boundary and auxiliary layer. These points are the nodes of the FEM mesh and the kinematic fields are obtained using the high order basis functions of SEM. No spatial interpolation is therefore needed at this interface, since a matching correspondence between SEM and FEM dofs is enforced.

(iii) On the FEM auxiliary layer boundary (Fig. 2b), impose nodal displacement field $\mathbf{u}$ and compute the traction vector solving the static problem with FEM. The traction vector defined on nodes is simply the nodal forces.

(iv) In the reduced domain (Fig. 2c), reconstruct the dynamic excitation from using the velocity field $\dot{\mathbf{u}}$ directly exported from SEM, and the nodal forces F_{node} computed previously with the FEM auxiliary layer (Fig. 2b)

3. Regional scale simulation and coupling verification

The present analysis focuses on the region of the Niigata prefecture in Japan where is located the Kashiwazaki-Kariwa nuclear power plant (KKNPP) facility. The area of interest considered for the numerical model is represented in Fig. 3, along with the location of the earthquake event, inspired by the 16/06/2007 aftershock - AS1 (in Fig. 3a) registered in the region.

A $48 \times 48 \times 23$ km^3 soil domain (auxiliary domain problem - $\mathcal{P}_0$) is numerically modeled in the spectral element code SEM3D [10, 11], using 8×10^6 hexahedral spectral elements. Five Gauss Lobatto Legendre (GLL) points are used for each direction, leading to a model size of 3×10^9 degrees of freedom (DoFs). A representation of the mesh is provided in Fig. 3b.

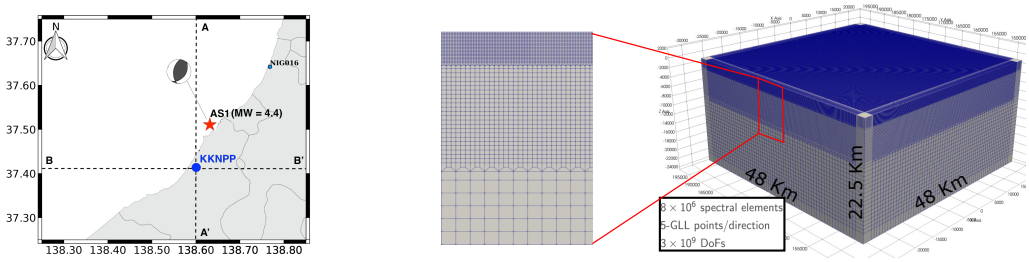

(a) Earthquake location. (b) Meshed soil domain.

Figure 3: Niigata region with borders of the SEM numerical model at the KKNPP site.

3.1. Regional 3D Geology

The geological profile used in this study consists of a complex regional geology model proposed by the Geological Survey of Japan (GSJ - [14]). It is an improvement of the previous NIED (National Research Institute for Earth Science and Disaster Prevention) model proposed by [15] for the Niigata area, based on several seismological observations.

A representation of the geological structure along the AA' "cut" (in Fig. 3a) is provided in Fig. 4. The regional scale representation is given in the left figure (Fig. 4a). In addition to this regional scale view of the geology, Fig. 4b presents a closer look (white box in Fig. 4a) at the region of the KKNPP facility in order to provide a better understanding of local geology. At the center of this "zoomed" version, the size of the FEM domain (reduced domain problem - $\mathcal{P}_1$) is provided. It is worth noticing, that the local scale FEM model ($520 \times 520 \times 190$ m^3) is around 100 times smaller in each direction than the regional scale one, something that showcases the multi-scale character of the SEM-FEM coupling.

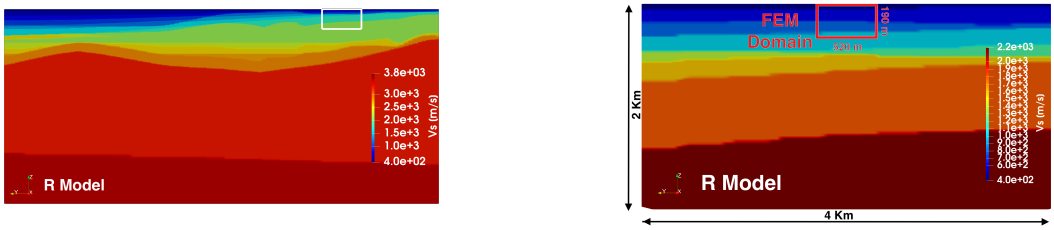

(a) Regional scale representation. (b) "Zoomed" version.

Figure 4: Shear wave velocity profile of the geological structure.

The corresponding mechanical linear isotropic characteristics of the FEM model of the reduced domain are provided in Table 1. Given the spatial variability of the mechanical properties, only the 1D profile along the Z direction and at the center of the reduced domain is given in this table. It is worth mentioning that in the current version of SEM3D there is no possibility to define a spatial variation of the attenuation parameters (Q_S, Q_P in Table 1). With this regard, a fixed value was chosen based on the mean value of the analysis presented in [16].

Table 1: 1D profile of mechanical parameters at the center of the FEM domain.

Geology	**Depth** [m]	ρ [m/s]	V_S [m/s]	V_P [m/s]	V_P/V_S [1]	Q_S [m/s]	Q_P [m/s]
R Model	-23	1990	400	1650	4.1	300	400
	-55	2000	500	1750	3.5	-	-
	-150	2050	600	1900	3.2	-	-
	-190	2060	700	2010	2.9	-	-

Material layers definition in SEM3D is defined here using a not-honoring approach (see also [17]), which means that a predefined mesh grid can be used. With this regard, given the minimum shear wave velocity of $V_{S_{min}} = 400\ m/s$, the minimum element size of $L_{min} = 80\ m$ and the 5-GLL points per direction, the numerical model is expected to provide valid results for a maximum frequency of $f_{max} = \frac{400}{80} = 5\ Hz$.

3.2. Dynamic excitation and boundary conditions

The present analysis considers the aftershock AS1 event with a hypocenter located on the north part of the KKNPP site, as presented in Fig. 3a. The aftershock event has a magnitude $M_{JMA} = 4.4$ (JMA stands for Japanese Meteorologic Agency), a hypocentral depth of 11 km, and a strike rake, and dip $(\phi_S; \lambda; \delta)$ of 187^o, 70^o, and 54^o respectively.

Simulation of the fault rupture in SEM3D is performed here using the Ruiz Integral Kinematic (RIK) source model, as it was proposed by [18]. It consists of an advanced kinematic-fractal model accounting for the generation of broadband signals via the fault rupture simulation. Source rupture is simulated as a series of multiple sub-events and each sub-event is modeled using circles the distribution of which is based on a fractal distribution describing the number-size relation.

Given the size-number relation, the next step lies in the definition of the slip distribution considered in the source model. The particular distribution of the RIK sub-sources is constrained by a spatial probability density function with respect to a predefined normalized slip model and

the total seismic moment defined for the seismic scenario. The slip model used to constrain the randomly generated slip for a new event can be obtained through an inversion process as in [18]. Nevertheless, in this case, a slip model for an earthquake of similar magnitude ($M_{JMA} = 4.4$) and the seismic context in Japan was directly retrieved from the literature [19].

The parameters used in order to generate the source model as well as the generated slip distribution are provided in Fig. 5. For a more detailed description concerning the RIK model and its particular configuration for the examined case, the reader should refer to [9].

Parameters	Values
Fault Dimensions	3.48 km × 3 km
Fault Discretisation	60 m × 60 m
Number of subsources	2900
Slip pulse width (L_0)	350 m
Rupture Velocity (V_R)	$0.8 \times V_S$

(a) Parameters of the source model.

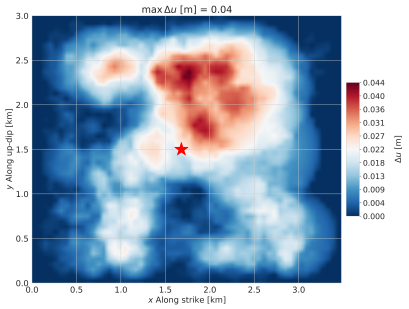

(b) Slip distribution.

Figure 5: Earthquake scenario generation based on the RIK model (reprinted by [9]).

Finally, Perfectly Matched Layers (PML) are used as absorbing boundary conditions in SEM3D in order to avoid spurious reflections on the boundaries.

3.3. Numerical Verification

The numerical verification of the presented SEM-FEM coupling is extensively discussed in [2], and is not the main objective of the presented work. Nevertheless, for reasons of completion, the comparison of the acceleration time histories between a full-SEM3D propagation and a SEM/FEM simulation and for several points at the surface of the reduced domain are provided in Fig. 6. According to this Fig. 6, an excellent correspondence is observed between the two approaches.

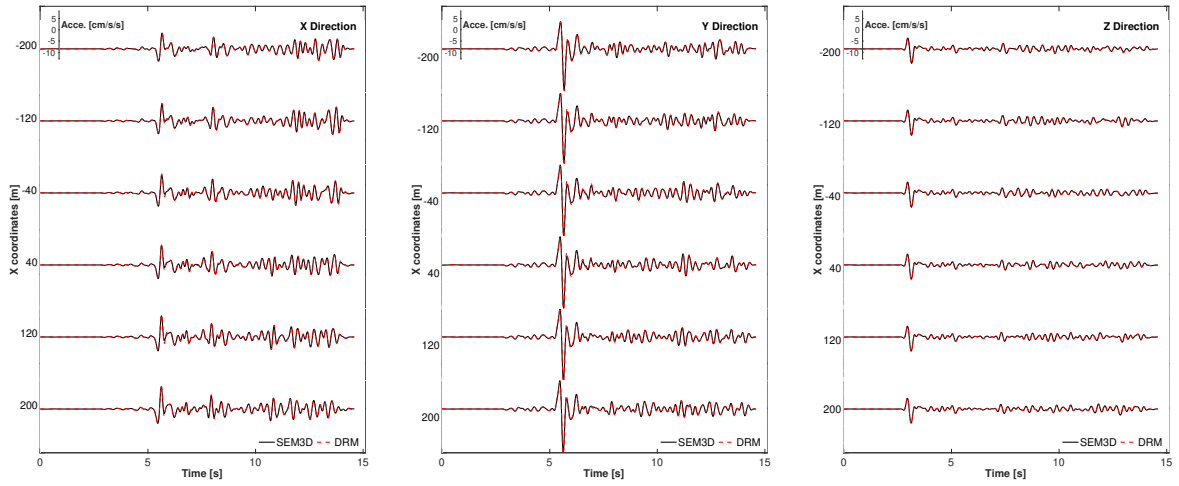

(a) X component. (b) Y component. (c) Z component.

Figure 6: Comparison of acceleration time histories at the surface of the reduced domain (drawn from [9]).

4. Towards a High-Performance Computing resolution with FEM

The case-study and the numerical verification of the coupling for the case of interest were presented in the previous section 3. In this section, the analysis focuses on the second step of the DRM approach and the adaptation of the finite element problem in a High-Performance Computing (HPC) framework.

4.1. The initial implementation of the coupling

The initial implementation of the SEM-FEM coupling [2] adopts the construction of the FEM model in a sequential sense, meaning that all the information concerning the discretized FEM domain, as well as the input excitation on the FEM boundary, is known by all MPI processes. Once the model is constructed, a parallel resolution of the dynamic system can be performed employing a direct parallel solver with *e.g.* MUMPS [20], or parallel iterative solvers with PETSc [21]. In other words, all the data are available on every process and only the elementary computations, assembly, and solution phases are done in parallel. This type of parallelism provides important advantages in terms of acceleration of the computational time highlighted in several engineering studies with code_aster.

Nevertheless, the current approach does not allow to efficiently utilize computational resources and becomes unfeasible in cases where physical problems with larger domains in terms of DoFs need to be numerically simulated. Such examples are the SSI analysis of whole nuclear island buildings or the multi-dimensional site-effect analysis including 3D realistic basins in a FEM framework in order to allow a better representation of several physical phenomena.

4.2. The adaptation of the coupling in a domain decomposition framework

In order to optimize the usage of computational resources, the coupling procedure was entirely revisited and adapted in a domain decomposition framework [5], where the whole domain is partitioned into several overlapping sub-domains and each sub-domain is processed separately by a MPI process. This partition includes the mesh of the reduced domain, as well as the input excitation field that needs to be defined on the boundary. As a result, each MPI process only knows information about the domain that is attributed to. Communications between sub-domains ensure the consistency of data on the overlapping "ghost layer" [22], where the exchange of information takes place between the traditional MPI communication process.

An example of the decomposition of the previous problem (see section 3) for 5 MPI processes is provided in Fig. 7. The partition of the mesh is given in Fig. 7a and each colored sub-domain is attributed to one MPI process. In a similar way, the partitioned input field (coming from the SEM3D simulation) is provided in Fig. 7b. It is worth noticing that, the partitioning of the input field, corresponds to the partitioning of the whole meshed domain. It can be seen through the presence of the one element overlapping "ghost layer" where the exchange of information takes place between the traditional MPI communication process in Fig. 7b.

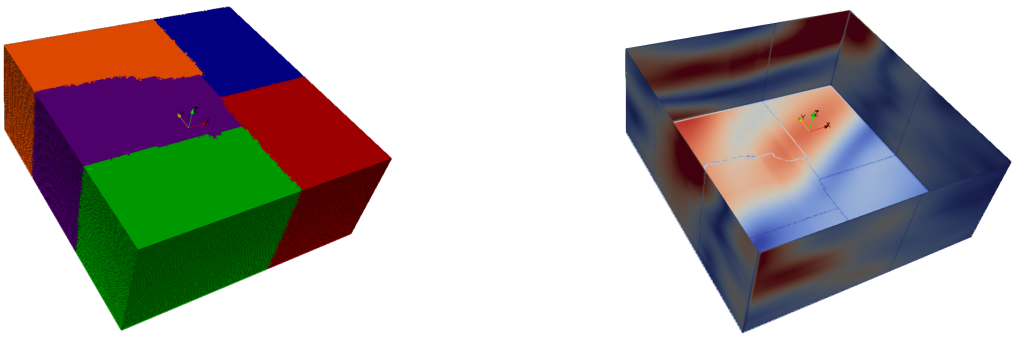

(a) Mesh partition. (b) Input field partition.

Figure 7: An example of the domain decomposition of the problem for 5 MPI processes.

4.3. Comparison between the different approaches

For illustration purposes, a comparison is provided here between different approaches in order to showcase the numerical performance of the HPC adaptation for the coupling. Three different cases are compared in this framework :

- **Sequential solution**: It consists of the initial version of the coupling in a sequential mode with 1 MPI process.
- **Parallel direct solver**: It consists of the initial version of the coupling and a parallel direct solver using MUMPS [20] for the dynamic resolution of the problem.
- **HPC resolution**: Solution based on the domain decomposition approach using iterative solvers based on PETSc [21]. The pre-conditioner used in this case is a simple precision factorization using MUMPS [20].

The FEM soil domain examined in section 3 is considered here for the comparison procedure. It is represented using 2×10^6 degrees of freedom, a size that allows an easy solution even for the sequential case.

Numerical performance is provided with Fig. 8 where the evolution of the computational time (CPU Time) is presented with respect to the number of the MPI processes considered for the solution of the dynamic problem. In Fig. 8, the purple dot corresponds to the sequential solution (2M DoFs for 1 MPI process), the red line corresponds to the parallel direct solver and the black line to the HPC resolution. The blue dots stand for the computation with 80 MPI processes, corresponding to 25K DoFs per MPI process.

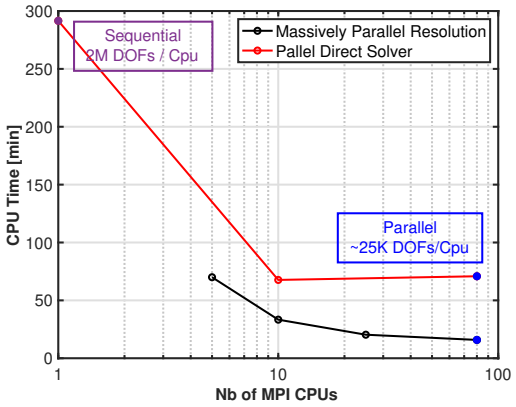

Figure 8: Evolution of the resolution CPU Time with respect to the number of MPI processes.

Main conclusions deriving from this Fig. 8 can be summarized as follows:

- The MUMPS direct parallel solver for 80 MPI processes takes around 1 h of CPU Time, which is $\times 5$ faster than the sequential solution. A "stagnation" of the CPU time is observed in this case as no important gains in CPU time can be observed between the solution with 10 MPI processes ($\approx$ 200K DoFs / MPI) and the one with 80 MPI processes ($\approx$ 25K DoFs / MPI). This can be justified from the saturation of the attributed memory for the numerical resolution.
- The HPC resolution for the same number of 80 MPI processes takes around 15 min, which is $\times 4$ faster than the parallel direct solver, and $\times 20$ faster than the sequential solution.
- A saturation of the CPU time is observed for the HPC resolution after 10 MPI processes. This can be explained from the fact that the size of the problem remains small and thus for a larger number of MPI processes the ratio of DoFs/MPI remains small.

5. Conclusions and perspectives

A SEM-FEM weak coupling for a more accurate definition of the seismic ground motion as an input excitation to soil-structure interaction or multi-dimensional site effect models in a FEM framework was discussed in this work. A brief verification of this coupling was presented for the case-study of the Niigata region where the KKNPP is located in Japan. Then the adaptation of the FEM solution in a massively parallel framework, which is the main focus of this paper was presented for the same case, presenting the important advantages of the newly implemented approach. In overall, the main conclusions can be summarized as follows:

- Optimization of the usage of numerical resources in terms of memory demands: Each MPI processor knows only information on mesh and field of sub-domain, and as a result memory demands are lower per MPI processor.
- Scalability of numerical performance to the available computational resources.
- Faster resolution of "traditional/trivial" problems compared to direct solver approaches. This stems mainly from the optimized manipulation of computational resources.
- Possibility to handle larger domains in terms of DoFs in a FEM framework.

The HPC resolution approach presents some important advantages, nevertheless some "caution" key points also need to be taken into consideration :

- Numerical performance depends on the efficiency of the data exchange between the two software. In this framework, further validation needs to be performed for larger problems.
- Numerical performance also depends on the pre-conditioner as not all pre-conditioner are adapted for the same type of physical simulation.
- Particular conditions, such as Lagrange multipliers also play a crucial role as they significantly reduce the performance of iterative solvers.

6. Acknowledgments

The presented work is part of the scientific activities supported by the Horizon 2020 METIS project and the SEISM Institut (https://www.institut-seism.fr/). The authors would also like to express their gratitude to the Association Nationale de la Recherche et de la Technologie (ANRT) for their financial support.

References

[1] Bielak J, Yoshimura C, Hisada Y, Fernández A. Domain Reduction Method for Three-Dimensional Earthquake Modeling in Localized Regions, Part I: Theory. Bulletin of the Seismological Society of America. 2003;93(2):825-40.

[2] Korres M, Lopez-Caballero F, Alves Fernandes V, Gatti F, Zentner I, Voldoire F, et al. Enhanced seismic response prediction of critical structures via 3D regional scale physics-based earthquake simulation. Journal of Earthquake Engineering. 2022:1-29.
[3] Code_Aster. General public licensed structural mechanics finite element software, included in the Salomé-Méca simulation platform. Website http://www.code-aster.org. En particulier : [R4.02.05] Éléments de frontière absorbante; 2017.
[4] Dolean V, Jolivet P, Nataf F. An Introduction to Domain Decomposition Methods: algorithms, theory and parallel implementation. France; 2015. Lecture. Available from: https://hal.science/cel-01100932.
[5] Tardieu N, Alves Fernandes V, Devesa G. Modélisation des effets de site multidimensionnels par le calcul haute-performance avec code_aster. In: 14ème Colloque National en Calcul de Structures. Giens (In French); 2019. .
[6] de Soza T, Sellenet N. HPC et calcul des structures : de la difficulté de rendre ultrascalable un code généraliste. In: 11e colloque national en calcul des structures, CSMA, May 2013, Giens, France; 2013. Available from: https://hal.science/hal-01717096/document.
[7] Gatti F, Touhami S, Lopez-Caballero F, Paolucci R, Clouteau D, Alves Fernandes V, et al. Broad-band 3-D earthquake simulation at nuclear site by an all-embracing source-to-structure approach. Soil Dynamics and Earthquake Engineering. 2018;115:263-80.
[8] Castro Cruz DA, Bertrand E, Julie R, Courboulex F. Apport des enregistrements sismologiques dans la prédiction du comportement non-linéaire des sols sous sollicitation sismique; 2019. Poster. Colloque de l'Association Française du Génie Parasismique.
[9] Korres M. Coupled 3D physics-based simulations for seismic source-to-structure response : Application to the Kashiwazaki-Kariwa nuclear power plant (Japan) case; 2021. PhD dissertation in Civil Engineering, Université Paris-Saclay 2021. Available from: http://www.theses.fr/2021UPAST118.
[10] SEM3D Registered at French Agency for Protection of Programs (Dépôt APP), CeCILL-C license. CEA, CentraleSupélec, IPGP and CNRS; 2017. Available from: https://github.com/sem3d/SEM.
[11] Touhami S, Gatti F, Lopez-Caballero F, Cottereau R, de Abreu Corrêa L, Aubry L, et al. SEM3D: A 3D High-Fidelity Numerical Earthquake Simulator for Broadband (0-10 Hz) Seismic Response Prediction at a Regional Scale. Geosciences. 2022;12(3). Available from: https://www.mdpi.com/2076-3263/12/3/112.
[12] Modaressi H, Benzenati I. Paraxial approximation for poroelastic media. Soil Dynamics and Earthquake Engineering. 1994;13(2):117-29.
[13] De Martin F, Modaressi H, Aochi H. Coupling of FDM and FEM in seismic wave propagation. In: 4th International Conference on Earthquake Geotechnical Engineering. Thessaloniki, Greece; 2007. .
[14] Sekiguchi H, Yoshimi M, Horikawa H, Yoshida K, Suzuki H, Matsuyama H, et al. 3D subsurface structure model of the Niigata sedimentary basin. Geological Survey of Japan—AIST annual report on active fault and paleoearthquake researches. 2009;9:175-259.
[15] Fujiwara H, Kawai S, Aoi S, Senna S, Ooi M, Matsuyama H, et al. A subsurface structure modeling of whole of Japan for strong-motion evaluation. In: 12th Japan Earthquake Engineering Symposium; 2006. p. 1466-9.
[16] Nakajima J, Matsuzawa T. Anelastic properties beneath the Niigata-Kobe Tectonic Zone, Japan. Earth, Planets and Space. 2017 12;69.
[17] Touhami S, Lopez-Caballero F, Clouteau D. A holistic approach of numerical analysis of the geology effects on ground motion prediction: Argostoli site test. Journal of Seismology. 2021;25(1):115-40.
[18] Gallovič F. Modeling Velocity Recordings of the Mw 6.0 South Napa, California, Earthquake: Unilateral Event with Weak High-Frequency Directivity. Seismological Research Letters. 2015 11;87(1):2-14.
[19] Ide S. Complex source processes and the interaction of moderate earthquakes during the earthquake swarm in the Hida-Mountains, Japan, 1998. Tectonophysics. 2001;334(1):35-54.
[20] Amestoy PR, Guermouche A, L'Excellent JY, Pralet S. Hybrid scheduling for the parallel solution of linear systems. Parallel computing. 2006;32(2):136-56.
[21] Balay S, Abhyankar S, Adams MF, Benson S, Brown J, Brune P, et al. PETSc/TAO Users Manual. Argonne National Laboratory; 2022. ANL-21/39 - Revision 3.18.
[22] Fan J, Nihei KT, Myer LR, Cook NG, Rector III JW. Overlap domain decomposition method for wave propagation. In: SEG Technical Program Expanded Abstracts 1997. Society of Exploration Geophysicists; 1997. p. 1485-8.